NASA Technical Memorandum 89841

Liquid Sheet Radiator

Donald L. Chubb and K. Alan White, III
Lewis Research Center
Cleveland, Ohio

Prepared for the
22nd Thermophysics Conference
sponsored by the American Institute of Aeronautics and Astronautics
Honolulu, Hawaii, July 8–10, 1987

NASA

LIQUID SHEET RADIATOR

Donald L. Chubb and K. Alan White, III
National Aeronautics and Space Administration
Lewis Research Center
Cleveland, Ohio 44135

E-3497

Abstract

A new external flow radiator concept, the liquid sheet radiator (LSR), is introduced. The LSR sheet flow is described and an expression for the length/width L/w, ratio is presented. A linear dependence of L/w on velocity is predicted that agrees with experimental results. Specific power for the LSR is calculated and is found to be nearly the same as the specific power of a liquid droplet radiator (LDR). Several sheet thicknesses and widths were experimentally investigated. In no case was the flow found to be unstable.

Nomenclature

A surface area

a_λ spectral absorption coefficient

d sheet thickness

f constant defied in Eq. (22)

g gravitational acceleration constant, 9.8 m/sec^2

i_λ black body intensity

L sheet length

ℓ length of slits

m mass of sheet

p pressure

p_λ spectral specific power

Q volume flow rate

q total emissive power

q_λ spectral emissive power

r_D radius of droplet in LDR

T temperature

t time

u x-direction velocity

v y-direction velocity

We Weber number, Eq. (15)

w slit width

x x-coordinate

y y-coordinate

z z-coordinate

γ constant defined by Eq. (12)

ϵ_λ spectral emittance

ϵ'_λ spectral emissivity

$\overline{\eta}$ average vignetting factor for LDR

λ wavelength

μ viscosity

ρ density

ρ_λ spectral reflectivity

σ surface tension

τ_λ spectral transmittance

Subscripts:

D refers to LDR

L refers to conditions at $y = L$

o refers to conditions at slit, $y = o$

s refers to LSR

w refers to slit width, w

Introduction

One way of significantly reducing the mass of a space radiator is to eliminate the containing walls for the working fluid. Thus the working fluid is exposed to the vacuum condition of space. Such an external flow radiator will have a lower mass than heat pipe or pumped loop type radiators. Ease of deployment and near immunity to micrometeoroid damage are two other important advantages of external flow radiators.

Currently, the liquid droplet radiator (LDR)[1-4] and the liquid belt radiator (LBR)[5-7] are the external flow radiators receiving the most research interest. In this paper a new external flow radiator, the liquid sheet radiator (LSR), is introduced. The LSR uses a thin ($\approx$100 μm) liquid sheet as the radiating surface. Similar to all external flow radiators, the working fluid of the LSR must be of very low ($\approx 10^{-8}$ torr) vapor pressure in order to keep evaporative losses low.

One of the advantages of the LSR is ease of design. Fabrication of narrow slits that are used in producing the sheet flow does not require precision machining techniques such as those necessary for fabricating the many small holes of a LDR. Also, the pump power required will be less since the viscous losses for a single slit will be less than the losses for many small holes. Collection of the liquid sheet flow is simplified since the sheet flow coalesces to a point (as will be discussed later). Thus only a small cross-sectional area collector, which does not have to contend with stream misalignment, is required.

The simpler design of the LSR sheet generator and collector should translate into lower mass for these components than for the LDR and LBR. In addition, as will be shown later, the specific power, p_{LSR}, for the sheet (power radiated/sheet mass) is approximately the same as the specific power, p_{LDR}, for a comparable droplet sheet.

In the next section the sheet flow geometry will be described and a simple analysis of this geometry will be presented. Following that, the specific power of the sheet will be compared with the specific power of a comparable droplet sheet. Then the preliminary experimental sheet flow results will be discussed and compared to the simple analysis. Finally, conclusions will be presented.

Liquid Sheet Geometry

A sketch of the flow geometry of a thin liquid sheet is shown in Fig. 1. As a result of surface tension forces at the edges of the sheet, cylinders are formed that grow in diameter in the flow direction, y. Connecting the edge cylinders and the rectangular portion of the sheet is a transition region, as shown in Fig. 1(b). This transition region will also grow in thickness in the flow direction. In order to satisfy the conservation of mass, the sheet width also decreases in the direction of flow. Finally the edge cylinders meet at some point $y = L$.

Determination of the exact shape of the sheet cross section requires the solution of the irrotational incompressible fluid equations (Laplace Eq.) with a moving boundary (sheet cross section). However, the critical scaling parameter for the LSR is the length/width ratio, L/w. To obtain a first approximation to this quantity the sheet cross section was assumed to consist of end cylinders plus a rectangular portion as shown in Fig. 1(c). Both the end cylinders and the rectangular portion grow in the flow direction. The analysis that follows includes the gravity force since the experiments to be discussed were performed in the Earth's gravity field.

Consider a coordinate system moving with the flow velocity, v, and a control volume determined by the edge cylinder as shown in Fig. 1(c). For conservation of momentum in the x-direction, rate of change of momentum in x-direction = force in x-direction

$$u(\rho u\, d\, dy) = (p_t - p_f) d\, dy \tag{1}$$

Where ρ is the fluid density, u is the x velocity and p_t is the surface tension pressure for a cylinder,[9]

$$p_t = \frac{\sigma}{r} \tag{2}$$

and σ is the surface tension, (N/m). For vacuum conditions, $p_f = 0$ so that Eqs. (1) and (2) yield the following:

$$u = \sqrt{\frac{\sigma}{\rho r}} \tag{3}$$

For the conservation of mass for the edge cylinder, increase in control volume mass = rate of mass addition

$$\rho(2\pi r)dr\, dy = \rho\, d\, u dt\, dy$$

$$\therefore \quad r\frac{dr}{dt} = \frac{ud}{2\pi} \tag{4}$$

Substituting (3) in (4) and integrating yields,

$$r = \left[\frac{5}{4}\frac{d}{\pi} t\sqrt{\frac{\sigma}{\rho}} + r_o^{5/2}\right]^{2/5} \tag{5}$$

Where $r = r_o$ at $t = 0$

For overall conservation of mass, the mass flow leaving the slit at $y = 0$ must equal the mass flow at $y = L$ where the end cylinders meet.

$$\rho w\, d_o v_o = 2\pi\rho v_L r_L^2 \tag{6}$$

Where v_o is the y velocity at $x = 0$, v_L is the y velocity at $y = L$ and r_L is the cylinder radius at $y = L$.

Substituting Eqs. (5) in (6) results in the following:

$$t_L\left(\frac{v_L}{v_o}\right)^{5/4} = \frac{2}{5}\sqrt{\frac{\rho}{\sigma}}\left(\frac{w\, d_o}{2\pi}\right)^{1/4}\frac{d_o}{d_L} w \tag{7}$$

Where, t_L is the time required for the flow to go from $y = 0$ to $y = L$ and d_L is the sheet thickness at $y = L$.

Since the gravitational field is in the y-direction.

$$v = gt + v_o \tag{8}$$

$$y = 1/2\ gt^2 + v_o \tag{9}$$

Where g is the gravitational acceleration constant (9.8 m/sec^2). From Eqs. (8) and (9) the following is obtained.

$$t = \frac{v_o}{g}\left[\sqrt{1+\gamma} - 1\right] \tag{10}$$

$$\frac{v}{v_o} = \sqrt{1+\gamma} \tag{11}$$

Where,

$$\gamma \equiv \frac{\text{gravitational potential energy}}{\text{kinetic energy}} = \frac{2gy}{v_o^2} \tag{12}$$

For the experimental conditions considered, $\gamma_w < 1$. Therefore, using Eqs. (10) and (11) in (7), to first order in γ_w the following solution is obtained for L/w.

$$\frac{L}{w} = \left(\frac{L}{w}\right)_{g=o}\left[1 - \frac{3}{8}\gamma_w\left(\frac{L}{w}\right)_{g=o}\right] \tag{13}$$

Where $(L/w)_{g=o}$ is the sheet length/width in gravity free conditions.

$$\left(\frac{L}{w}\right)_{g=o} = \frac{2}{5}\left(\frac{d_o}{d_L}\right)_{g=o}\sqrt{\frac{\rho}{\sigma}}\left(\frac{w\,d_o}{2\pi}\right)^{1/4} v_o \qquad (14a)$$

$$= \frac{2}{5}\left(\frac{d_o}{d_L}\right)_{g=o}\left(\frac{w}{2\pi\, d_o}\right)^{1/4}\sqrt{We} \qquad (14b)$$

and We is the Weber number

$$We \equiv \frac{d_o \rho}{\sigma} v_o^2 \qquad (15)$$

and

$$\tau_w = \frac{2gw}{v_o^2} \qquad (16)$$

For the zero gravity conditions Eq. (14a) shows that $(L/w)_{g=o}$ should be a linear function of velocity, v_o, if d_L is independent of v_o. When $g \neq o$ Eq. (13) shows that L/w is not a linear function of v_o since $\tau_w \sim 1/v_o^2$. Also, when $g=o$ Eq. (14a) indicates $(L/w)_{g=o}$ is a weak function ($\sim w^{1/4}$) of w provided d_L is independent of w. For sufficiently wide sheets (large w) the sheet thickness, d_L, should be independent of w.

The $(L/w)_{g=o}$ ratio is shown in Fig. 2 as a function of Weber number. Results are shown for $(d_o/d_L)_{g=o}(w/d_o)^{1/4} = 1, 2, 4$. In the case of the LSR, We ≈ 200 and for a laboratory experiment $(d_o/d_L)_{g=o}(w/d_o)^{1/4} \approx 2$ while for a full scale LSR $(d_o/d_L)_{g=o}(w/d_o)^{1/4}$ may be as large as 4. Thus, Fig. 2 yields $L/w \approx 7$ for a lab experiment and $L/w \approx 14$ for a full scale LSR.

Stability of the sheet flow is a critical issue for the LSR. In the laboratory experiments to date, there has been no indication of the sheet flow becoming unstable. However, for a full scale LSR flow stability may still be a problem. Currently a theoretical stability analysis is being carried out. Results of that analysis will be reported at a later date.

Specific Power of Sheet

The large surface area to volume ratio for spherical droplets results in large specific powers for a droplet sheet.[1,2] However, as will be shown below, for the same fluid a continuous sheet will have approximately the same specific power as a droplet sheet.

In the following analysis for the sheet emissive power a constant thickness sheet is assumed. As previously pointed out, the sheet grows in thickness in the flow direction. Therefore, since the sheet emittance (Eq. (A-12)) increases with thickness, the constant thickness emissive power calculated will be less than the actual emissive power. As a result, the sheet specific power presented here should be a conservative estimate of the actual specific power.

In Appendix A, an expression for the emissive power of an infinite sheet of constant thickness, d_o, surrounded by a black body source of radiation at temperature, T_∞, is developed. Assuming that $\tau_\lambda \rho_\lambda << 1$, where τ_λ is the sheet transmittance (Eq. (A-11)) and ρ_λ is the reflectivity of the sheet-vacuum interface, then the spectral emissive power is

$$q_{\lambda_s} = \pi\left(1 - \rho_{\lambda_s}\right)\epsilon_{\lambda_s}\left[i_\lambda(T) - i_\lambda(T_\infty)\right] \qquad (17)$$

where i_λ is the black body intensity, (Eq. (A-2)) and ϵ_{λ_s} is the sheet spectral emittance (Eq. (A-12)).

Define the spectral specific power as follows:

$$p_{\lambda_s} \equiv \frac{\text{power emitted/wavelength}}{\text{mass of sheet}} = \frac{2A_s q_{\lambda_s}}{m_s} \qquad (18)$$

Experimentally it was found that the sheet area is triangular in shape, $A_s = wL/2$.

For constant sheet flow velocity,

$$m_s = \rho w L\, d_o \qquad (19)$$

where ρ is the density, w is the sheet width, L is the sheet length and d_o is the sheet thickness at the slit. Equation (19) holds for both variable and constant thickness sheets. Using Eqs. (17) and (19) in (18) yields the following result.

$$p_{\lambda_s} = \pi\left(1 - \rho_{\lambda_s}\right)\frac{\epsilon_{\lambda_s}}{\rho\, d_o}\left[i_\lambda(T) - i_\lambda(T_\infty)\right] \qquad (20)$$

From Ref. 2 the spectral emissive power of the droplet sheet can be written as,

$$p_{\lambda_D} = \pi f\left[i_\lambda(T) - i_\lambda(T_\infty)\right] \qquad (21)$$

where f = emissivity/(mass/area). The f factor is written in terms of f for an individual drop, f_D, and the average vignetting factor $\bar{\eta}$,

$$f = \bar{\eta} f_D \qquad (22)$$

$$f_D = \frac{3\epsilon'_{\lambda D}}{\rho r_D} \qquad (23)$$

Where ϵ'_{λ_D} is the drop spectral emissivity and r_D is the drop radius. The optimum LDR of Mattick and Hertzberg[2] has $\bar{\eta} \approx 1/2$. Therefore, Eq. (21) becomes the following:

$$p_{\lambda_D} = \frac{3\epsilon'_{\lambda_D}}{2\rho r_D}\pi\left[i_\lambda(T) - i_\lambda(T_\infty)\right] \qquad (24)$$

For both the droplet sheet and the continuous sheet operating at the same temperature, Eqs. (20) and (24) yield the following.

$$\frac{p_{\lambda_S}}{p_{\lambda_D}} = \frac{2}{3}\left(\frac{r_D}{d_o}\right)\left(\frac{\epsilon_{\lambda_S}}{\epsilon'_{\lambda_D}}\right)\left(1 - \rho_{\lambda_S}\right) \qquad (25)$$

Similar to the analysis for the emissive power of an infinite sheet in Appendix A, analysis of a sphere yields, (assuming $\tau_{\lambda_D}\rho_{\lambda_D} << 1$ and $i_\lambda(T_\infty) = 0$).

$$q_{\lambda_D} = \pi\left(1 - \rho_{\lambda_D}\right)\epsilon_{\lambda_D} i_\lambda(T) \qquad (26)$$

Where ρ_{λ_D} is the reflectivity at the sphere surface-vacuum interface and ϵ_{λ_D} is the sphere emittance[10] given in terms of the absorption coefficient, a_λ, as follows:

$$\epsilon_{\lambda_D} = 1 - \tau_{\lambda_D} = 1 - \frac{2}{\left(2a_\lambda r_D\right)^2}\left[1 - \left(2a_\lambda r_D + 1\right)e^{-2a_\lambda r_D}\right] \qquad (27)$$

Therefore, the emissivity of the sphere is the following:

$$\epsilon'_{\lambda_D} \equiv \frac{q_\lambda}{\pi i_\lambda(T)} = \left(1 - \rho_{\lambda_D}\right)\epsilon_{\lambda_D} \qquad (28)$$

For maximum specific power of the LSR, d_o should be as small as possible (see Eq. (20)). Similarly, for the LDR, r_D should be as small as possible. Therefore, the approximations $a_\lambda d_o << 1$ and $2a_\lambda r_D << 1$ can be made in Eqs. (A-12) and (28) so that to first order in $a_\lambda d_o$ and $2a_\lambda r_D$,

$$\frac{\left(1 - \rho_{\lambda_S}\right)\epsilon_{\lambda_S}}{\epsilon'_{\lambda_D}} \approx \frac{3}{2}\left[\frac{1 - \rho_{\lambda_S}}{1 - \rho_{\lambda_D}}\right]\frac{d_o}{r_D} \qquad (29)$$

Using Eq. (29) in Eq. (25) and assuming $\rho_{\lambda_D} = \rho_{\lambda_S}$ yields the following result:

$$\frac{p_{\lambda_S}}{p_{\lambda_D}} \approx 1 \qquad (30)$$

Since this result is wavelength independent, it also applies to the total specific power ratio, $\left(\text{total specific power} = \int_0^\infty p_\lambda\, d\lambda\right)$. Equation (30) shows that the continuous sheet specific power is approximately the same as the droplet sheet specific power.

As pointed out in the introduction, the design advantages of the LSR should translate into lower mass for the sheet generator and collector than for the generator and collector of a comparable LDR. Therefore, since the specific power of a continuous sheet is nearly the same as a droplet sheet, the overall mass of the LSR should be less than a comparable LDR.

Experimental Liquid Sheet Results

In order to test the validity of the analytical predictions outlined in Eqs. (1) to (14), an experimental investigation of liquid sheet flow and stability was conducted. The main elements of the apparatus used are shown in Fig. 3. The liquid sheet generator consists of a cylindrical cavity 6.4 cm in inner diameter and 5.1 cm in length, which is mounted in a vacuum bell jar. Bottled nitrogen is used to force the test liquid from a liquid reservoir (not shown) to the generator head and through a slit at the bottom of the generator head. The sheet thus formed flows downward in a 5 to 10 μm Hg vacuum environment (maintained by a mechanical pump), and is collected in a container at the bottom of the bell jar. The flow loop does not allow for continuous operation; when the fluid reservoir is depleted, the test liquid is transferred back from the collector.

A diffusion pump oil, Dow Corning 704 (tetramethyltetraphenyltrisiloxane), was used for the experiments. Since the vapor pressure of DC-704 at room temperature is four orders of magnitude lower than the background pressure, vaporization of the sheet is insignificant. Any aerodynamic drag on the sheet at this vacuum level is also negligible.

The slits used to form the sheets were fabricated in 50.8 mm diameter brass disks. The disks were nominally 6.3 mm thick, and were supported by the lower flange of the generator head, which was bolted to the bottom of the generator cavity. The thickness of the brass disk, and the method of supporting them, insured that the slits did not deform even with pressure drops across the slit of 130 psi. This experimental observation was verified by calculating the deflection of a plate under load. The slit geometry is illustrated in Fig. 4, which shows a perspective view of the slit and disk, obtained by slicing the disk into two symmetrical halves. The slit has a width, w, a thickness, d_o, and a length, ℓ. A 90° taper to the slit length enables low ℓ/d's to be milled, while simultaneously preserving the dimensional integrity of the slit. Ten different slits were examined experimentally: for each of three widths (16.5, 25.4, and 34.3 mm), slits of nominal thicknesses of 50, 75, and 100 μm and nominal ℓ/d of 1.0 were tested. A slit 34.3 mm wide, 100 μm thick, and with an ℓ/d of 3.44, was also investigated.

For each of the ten slits, sheets of variable length were formed by varying the sheet velocity over the largest range achievable by the apparatus. The minimum sheet velocity was that at which the shortest sheet could be formed; below the flow rate corresponding to this minimum velocity, the test liquid oozed from the slit, but did not form a continuous sheet. The sheets were photographed on 35 mm Kodak Plus-X film, using a 50 mm wide angle lens. The sheet was back lighted, such that the light was diffused through opal (translucent) glass to form a shadowgraph of the sheet on the film. The sheet was thus uniformly illuminated, except near its emergence from the generator head.

The velocity of the sheet was calculated from a known flow rate, Q.

$$v_o = \frac{Q}{w\, d_o} \qquad (31)$$

The flow rate was determined from an accurate calibration of each slit, effected by collecting and weighing the effluent liquid for a length of time. This process was repeated for a sufficient number of Δp, Q pairs to establish the calibration. The pressure drop, Δp, across the slit was determined by a static transducer, and the temperature of the fluid by a thermocouple, the two being located inside the generator head as close to the slit as practical. As the viscosity of DC-704 is a strong function of temperature, it was necessary to correct even for 1 to 2 °C temperature variations. The analog of the Hagen-Poiseuille law for flow through a narrow slit is,[11]

$$Q = \frac{\Delta p\, d_o^3 w}{12\, \mu \ell} \qquad (32)$$

Thus, the $Q\mu$ product was plotted as a function of Δp, allowing calculation of flow rates at temperatures other than the calibration temperature. All experimental work was at a temperature of 20 to 29 °C. Since the ℓ/d_o ratios for the slits were small, flow through the slits was not necessarily fully-developed, and Q was not linear with Δp. The calibration curve was well fit by a third order polynomial, with correlation coefficients of 0.99 or better.

Examination of more than 250 photographs revealed that highly stable sheets were always formed, which confirmed an analytical prediction (to be published) of sheet stability in this flow regime. In other flow regimes, liquid sheets separate into ligaments, which in turn break up into droplets[12-14] due to Rayleigh and Taylor instabilities. (Atomization of a liquid sheet, as discussed in Refs. 12 to 14, is employed for a number of end uses, notably heterogeneous combustion.) Vibrations from the mechanical vacuum pump, which were imparted to the generator head, are sufficient to break up a cylinder into droplets, due to Rayleigh instabilities.[4,8] However, neither these vibrations, nor the ultrasonic and acoustic oscillations of a piezoelectric crystal immersed in the DC-704 inside the generator head, caused any detectable instabilities in the sheet. The sheet thus appears stable to a wide frequency range of imparted disturbances.

The behavior of the sheet was strongly dependent on the slit geometry. The fluid dynamics of the sheet after convergence at length L varied considerably with changes in the slit geometry, and also with the sheet velocity. These parameters also greatly influenced the manner in which the sheet converged in the convergence length, L. In some cases, the decrease in sheet width was accomplished solely by formation of cylinders on the sheet edges, as described earlier in this paper. In other instances, for certain sheets having an ℓ/d_o of 1.0, a reduction in sheet width was accompanied by a twisting of the sheet as much as 180° about the plane containing the slit and initial portion of the sheet. This twisting occurred over the entire length for which the sheet could be observed, both before and after the convergence length L. This twisting was observed for all three 34.3 mm wide slits, as well as for the 25.4 mm slit of 75 μm thickness. When the ℓ/d_o ratio was increased to 3.44, the sheet remained in one plane, regardless of velocity.

Of the ten slits examined, the slit with an ℓ/d_o of 3.44 behaved most ideally, although sheets from all ten slits were very stable over the entire velocity range investigated. The longer ℓ/d_o slit most likely yielded the most ideal sheets due to the near establishment of fully-developed laminar flow through the slit. Three additional slits having ℓ/d_o ratios of 7, 10 and 12.5 were also tested. Flow through these slits was observed, and flow behavior identical to that of the 3.44 ℓ/d_o slit was noted.

Difficulty in obtaining a sheet with a width equal to that of the slit was occasionally observed. In such instances, the fluid would form into two or three narrower sheets along the width of the slit. These sheets would converge independently of each other. Flow behavior of these undesired sheets was the same as for a single sheet formed from a slit. Proper ultrasonic cleaning of the slit eliminated this anomaly whenever it was observed, with the desired sheet formation then resulting.

Representative photos of the sheets observed are shown in Figs. 5(a) to (c). As can be seen, the sheets are very nearly perfect isosceles triangles. Figure 5 shows a sheet with an L/w ratio of 9.6, and Fig. 5(b) shows a sheet with one of 1.5. Although difficult to observe, when these sheets were examined at 4x projection, both sheets were noted to be slightly convex. Sheets from the other nine slits, such as the sheet of Fig. 5(c), were all slightly, almost imperceptibly, concave. The behavior of the sheet after the convergence length, L, which is of limited concern for the LSR concept, is shown in Fig. 5(c) as contrasted to Figs. 5(a) and (b). The sheet of Fig. 5(c) is observed to degenerate after convergence into diverging fluid jets, which subsequently break up into droplets due to Rayleigh instabilities. The behavior seen in Figs. 5(a) and (b) is typical of the majority of sheets observed. Sheet behavior such as shown in Fig. 5(c) is only of concern for off-design LSR performance, when the sheet length L might not match the distance between the sheet generator and sheet collector.

The dependence of sheet length upon velocity is shown in Figs. 6(a) to (c). Sheet width is a constant for each plot, with sheet thickness as a parameter. The plots show the experimental data, with the least-squares line obtained from a one-paramenter curve fit of the data. As can be seen, the fit is very good. The linear relation between sheet length and velocity agrees with the theoretical prediction of Eq. (14). Each figure also shows an increase in sheet length (at any velocity) with increasing sheet thickness, d_o. It will be further noticed in Fig. 6(c) that the ℓ/d_o ratio of the slit affected the functional relation between sheet length velocity thickness and width. As discussed above, sheet behavior was visually observed to be strongly influenced by slit ℓ/d_o. Hence, the functional dependence on slit ℓ/d evidenced in Fig. 6(c) is to be expected.

Comparison of Theoretical and Experimental Flow Results

The experimental results for L/w indicate a linear dependence on the velocity, v_o. This is in agreement with the theoretical prediction, Eq. (14) if d_o/d_L is independent of v_o and $\gamma_w << 1$ (for all experimental conditions $\gamma_w < 0.1$). For sufficiently wide slits, d_o/d_L should be independent of w. In that case, according to Eq. (14), $L/w \sim w^{1/4}$. Only three slit widths were experimentally investigated. Therefore, there is insufficient data to determine L/w as a function of w. However, in comparing the $w = 25.4$ mm and $w = 34.2$ mm data it is found that $L/w \sim w^{1/4}$ for the $d_o = 50$ μm and 100 μm slits. The $w = 16.5$ mm slits data does not agree with $L/w \sim w^{1/4}$. In this case d_o/d_L probably is a function of w since w is not large enough to make end effects negligible. Also, in comparing the $d_o = 75$ μm slits at $w = 25.4$ mm and $w = 34.2$ mm we find that the $L/w \sim w^{1/4}$ relation does not apply. More experimental data of L/w as a function of w is necessary to determine the relation between L/w and w. However, it can be concluded that L/w is a slowly varying function of w for sufficiently wide slits.

Assuming the simple theoretical result (Eq. (14)) is correct, then the experimental linear dependence of L/w on v_o implies that d_o/d_L is independent of v_o. Also, as discussed above, d_o/d_L is independent of w. However, using Eq. (14) and the experimental data we find that d_o/d_L is an increasing function of d_o. Since only three slit thicknesses were tested there is insufficient data to determine the relation between d_o/d_L and d_L. A more complete analysis that predicts the shape of the sheet cross section will also establish the relationship between d_o/d_L and d_o.

Finally, experimental results for L/w indicate a dependence on the slit length/thickness ratio, ℓ/d_o. As Fig. 6(c) shows, the $\ell/d_o = 3.44$ slit yields a larger L/w than the $\ell/d_o = 1.0$ slit. The twisting of the sheet observed with $\ell/d = 1.0$ slits indicates a velocity component in the Z-direction. Since the twisting did not occur with the $\ell/d = 3.44$, 7, 10, 12.5 slits only x and y velocity components exist. Future work will use the larger ℓ/d slits to remove the unwanted z velocity component.

Conclusion

Preliminary theoretical and experimental results for a liquid sheet radiator (LSR) are encouraging. The specific power of the LSR is calculated as approximately the same as that of the liquid droplet radiator (LDR) sheet. Therefore, the simpler design for the LSR sheet generator and collector should result in a higher specific power for the LSR total system than for the LDR total system. Also, the LSR should not have the alignment problems associated with the many (10^5-10^6) droplet streams of the LDR.

The experimental flow results indicate very stable sheet flows. Also, the experimental linear dependence of L/w on velocity, v_o, is in agreement with the simplified analysis. More experimental data is necessary to determine L/w as a function of slit width, w, and thickness, d_o. Preliminary experimental results for L/w versus w show agreement with the theoretical $L/w \sim w^{1/4}$ result.

Further experimental work should be directed at determining the sheet cross-sectional shape, and the sheet emissivity.

Appendix A -

Emissive Power of Continuous Sheet

Consider an infinite sheet of thickness, d_o, in a vacuum and receiving black body intensity $i_\lambda(T_\infty)$ as shown in Fig. 1(a). Make the following approximations:

1. Absorption coefficient, a_λ is constant across the sheet and no scattering,
2. Sheet at constant temperature, T,
3. Vacuum-sheet interface behaves in a diffuse manner with reflectivity, ρ_λ

$$\pi i_\lambda^-(d_o,\theta) = \rho_\lambda q_{\lambda_i}(d_o) + (1 - \rho_\lambda) q_{\lambda_\infty}$$

$$\pi i_\lambda^+(0,\theta) = \rho_\lambda q_{\lambda_i}(o) + (1 - \rho_\lambda) q_{\lambda_\infty}$$

With these approximations, the intensity moving in the positive z-direction, $i_\lambda^+(z,\theta)$ is given by[10]

$$i_\lambda^+(z,\theta) = i_\lambda^+(o,\theta) e^{\frac{-a_\lambda z}{\cos\theta}} + i_\lambda(T)\left[1 - e^{\frac{-a_\lambda z}{\cos\theta}}\right] \tag{A-1}$$

where the black body intensity, $i_\lambda(T)$ is the following:

$$i_\lambda(T)d\lambda = \frac{2C_1\, d\lambda}{\lambda^5 (e^{c_2/\lambda T} - 1)} \tag{A-2}$$

$$C_1 = hC_o^2 = 0.595\times10^8 \frac{\text{WATTS } \mu m^4}{m^2} \tag{A-3}$$

$$C_2 = \frac{hC_o}{k} = 14\,388 \ \mu m\ K \tag{A-4}$$

Where C_o is the vacuum speed of light, h is Planck's constant and k is the Boltzmann constant.

Referring to Fig. A-1, the spectral emissive power of the sheet is

$$q_\lambda = q_{\lambda_o}(d_o) - q_{\lambda_\infty} = (1 - \rho_\lambda)\left[q_{\lambda_i}(d_o) - q_{\lambda_\infty}\right] \tag{A-5}$$

Since the vacuum radiation is assumed to be black body,

$$\pi i_\lambda(T_\infty) = q_{\lambda_\infty} \tag{A-6}$$

From symmetry,

$$i_\lambda^-(d_o,\theta) = i_\lambda^+(o,\theta) \qquad (A-7)$$

Therefore, using Eqs. (A-6), (A-7) and approximation 3 in Eq. (A-1) for $z = d_o$ yields the following.

$$i_\lambda^+(d_o,\theta) = \left[\frac{\rho_\lambda}{\pi} q_{\lambda_i}(d_o) + (1-\rho_\lambda) i_\lambda(T_\infty)\right] \times e^{\frac{-a_\lambda d_o}{\cos\theta}} + \left[1 - e^{\frac{-a_\lambda d_o}{\cos\theta}}\right] i_\lambda(T) \qquad (A-8)$$

The incident power at $z = d_o$, $q_{\lambda_i}(d_o)$ is the following:

$$q_{\lambda_i}(d_o) = \int_{\psi=0}^{2\pi}\int_{\theta=0}^{\pi} i_\lambda^+(d_o,\theta)\cos\theta\sin\theta\, d\theta\, d\psi \qquad (A-9)$$

Substituting Eq. (A-8) in (A-9) and carrying out the integrations yields the following:

$$q_{\lambda_i}(d_o) = \frac{\pi}{1-\tau_\lambda\rho_\lambda}\left[(1-\rho_\lambda)\tau_\lambda i_\lambda(T_\infty) + \epsilon_\lambda i_\lambda(T)\right] \qquad (A-10)$$

where τ_λ is the sheet spectral transmittance, and ϵ_λ is sheet spectral emittance or spectral absorptance,

$$\tau_\lambda = 2E_3(a_\lambda d_o) \qquad (A-11)$$

$$\epsilon_\lambda = \alpha_\lambda = 1 - \tau_\lambda = 1 - 2E_3(a_\lambda d_o) \qquad (A-12)$$

$$E_n(x) = \int_0^1 \mu^{n-2} e^{-x/\mu} du \text{ - Exponential Integral} \qquad (A-13)$$

Substitution of Eq. (A-10) in (A-5) gives the following result for the spectral emissive power of the sheet.

$$q_\lambda = \frac{\pi(1-\rho_\lambda)}{1-\tau_\lambda\rho_\lambda}\epsilon_\lambda\left[i_\lambda(T) - i_\lambda(T_\infty)\right] \qquad (A-14)$$

If the sheet absorption coefficient, a_λ, and reflectivity, ρ_λ, are independent of wavelength then the total emissive power is the following:

$$q = \int_0^\infty q_\lambda d\lambda = \frac{\sigma\epsilon(1-\rho)}{1-\tau\rho}\left[T^4 - T_\infty^4\right] \qquad (A-15)$$

where $\sigma(= 5.67\times10^{-8}$ WATTS/m^2 K^4) is the Stefan-Boltzmann constant.

Acknowledgements

The authors wish to acknowledge Al Blaze, David Cockran, Peter Klein, William Parkinson, Charles Smalley, and Barry Stephenson, for their special assistance in conducting the experimental work.

REFERENCES

1. Mattick, A.T. and Hertzberg, A., "Liquid Droplet Radiators for Heat Rejection in Space," Journal of Energy, Vol. 5, No. 6, Nov.-Dec. 1981, pp. 387-393.

2. Mattick, A.T. and Hertzberg, A., "Liquid Droplet Radiator Technology Issues," Space Nuclear Power Systems 1984, Vol. 1, M.S. El-Genk and M.D. Hoover, Eds., Orbit Book Co., Malabar, FL, 1984, pp. 427-435.

3. Brown, R.F. and Kosson, R., "Liquid Droplet Radiator Sheet Design Considerations," Advanced Energy Systems - Their Role in Our Future, Vol. 1, American Nuclear Society, LaGrange Park, IL, 1984, pp. 330-338.

4. Presler, A.F., Coles, C.E., Diem-Kinsop, P.S., and White, K A. III, "Liquid Droplet Radiator Program at the NASA Lewis Research Center," ASME Paper 86-HT-15, June 1986.

5. Weatherston, R.C. and Smith, W.E., "A Method for Heat Rejection from Space Power Plants," American Rocket Society Journal, Vol. 30, No. 3, Mar. 1960, pp. 268-269.

6. Knapp, K., "A Study of Moving Belt Radiators for Heat Rejection in Space," AFRPL-TR-84-001 Air Force Rocket Propulsion Laboratory, Jan. 1984.

7. Teagan, W.P. and Fitzgerald, K., "Preliminary Evaluation of a Liquid Belt Radiator for Space Applications," NASA CR-174807, 1984.

8. Muntz, E.P. and Dixon, M,, "The Characteristics, Control and Uses of Liquid Streams in Space," AIAA Paper 85-0305, Jan. 1985.

9. Batchelor, G.K., An Introduction to Fluid Dynamics, Cambridge University Press, 1967, pp. 63-64.

10. Siegel, R. and Howell, J.R., Thermal Radiation Heat Transfer, second edition, Hemisphere Publishing Corp., Washington, D.C., 1981, pp. 464, 611.

11. Bird, R.B., Stewart, W.E., and Lightfoot, E.N., Transport Phenomena, John Wiley and Sons, New York, 1960.

12. Dombrowski, N. and Johns, W.R., "The Aerodynamic Instability and Disintegration of Viscous Liquid Sheets," Chemical Engineering Science, Vol. 18, No. 3, Mar. 1963, pp. 203-214.

13. Nakayama, M. and Takahashi, Y., "Experimental and Theoretical Investigation of Longitudinal Vibrations on Liquid Jets and Sheets," Proceedings of the 2nd International Conference on Liquid Atomization and Spray Systems, (ICLASS '82), University of Wisconsin, Madison, WI, 1982, pp. 1-8.

14. Arai, T. and Hashimoto, H., "Disintegration of a Thin Liquid Sheet in a Cocurrent Gas Stream," Proceedings of the 3rd International Conference on Liquid Atomization and Spray Systems, (ICLASAA '85), Istitute of Energy, London, England, 1985, pp. VI B-1-1 to VI B-1-7.

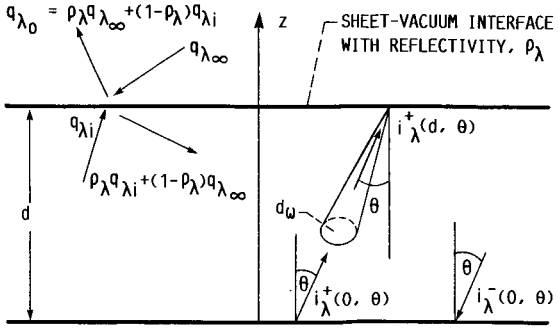

FIGURE A1. - SCHEMATIC OF INFINITE SHEET RADIATION.

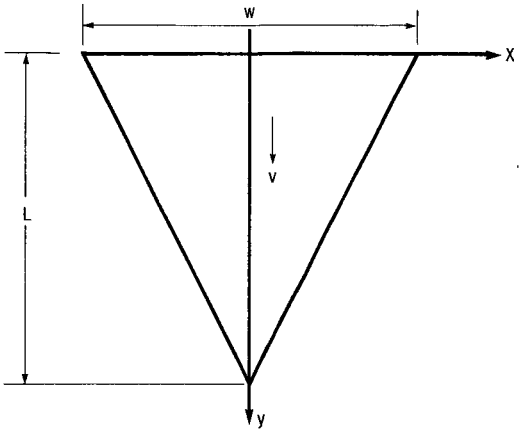

(A) TOP VIEW OF SHEET FLOW.

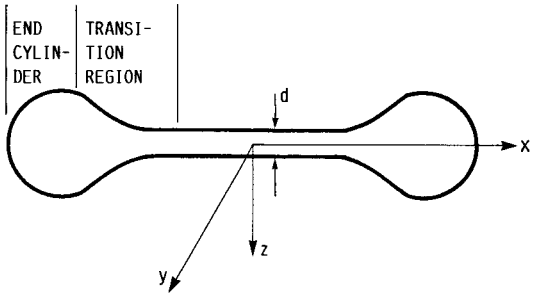

(B) CROSS-SECTION OF SHEET FLOW.

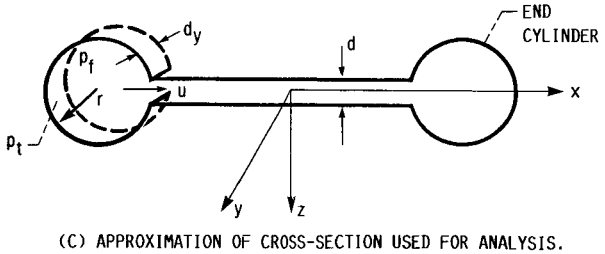

(C) APPROXIMATION OF CROSS-SECTION USED FOR ANALYSIS.

FIGURE 1. - SCHEMATIC OF THIN LIQUID SHEET FLOW.

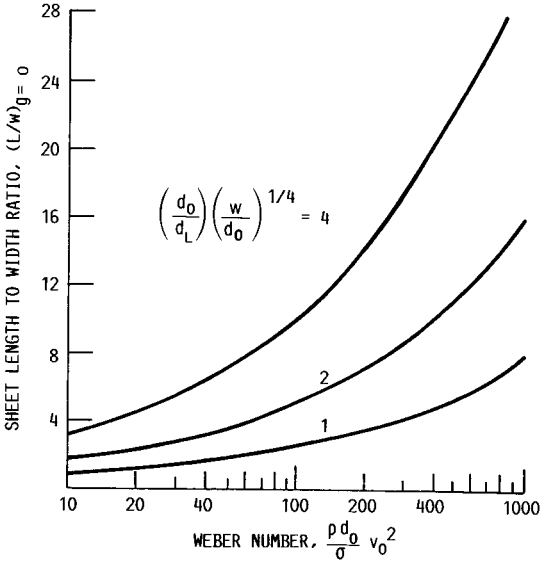

FIGURE 2. - DIMENSIONLESS SHEET LENGTH FOR ZERO GRAVITY ($Y_w = 0$).

ORIGINAL PAGE IS
OF POOR QUALITY

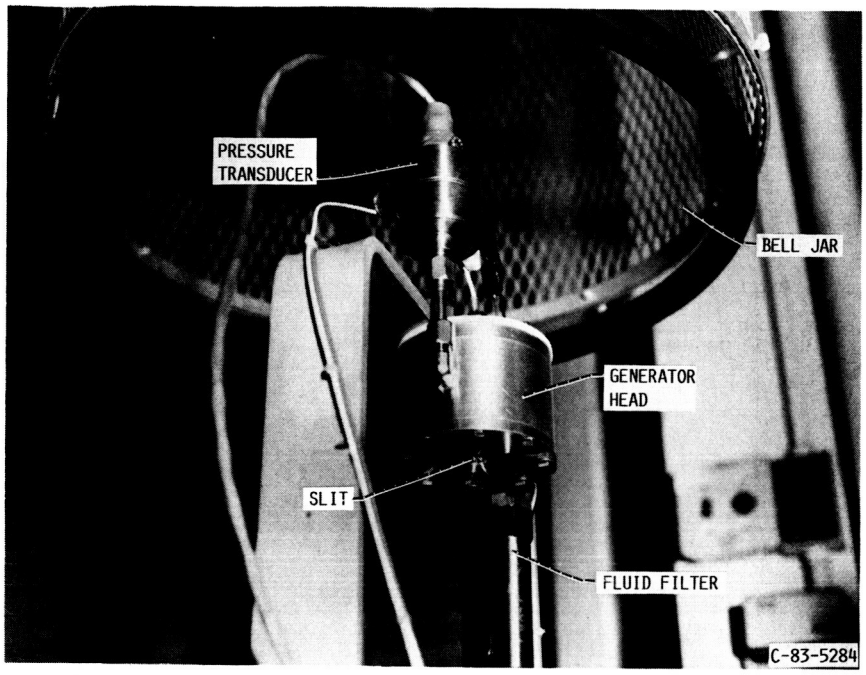

FIGURE 3. - EXPERIMENTAL LIQUID SHEET GENERATOR.

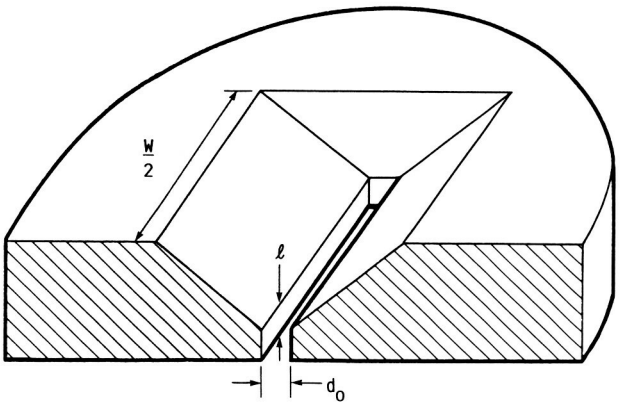

FIGURE 4. - SLIT GEOMETRY.

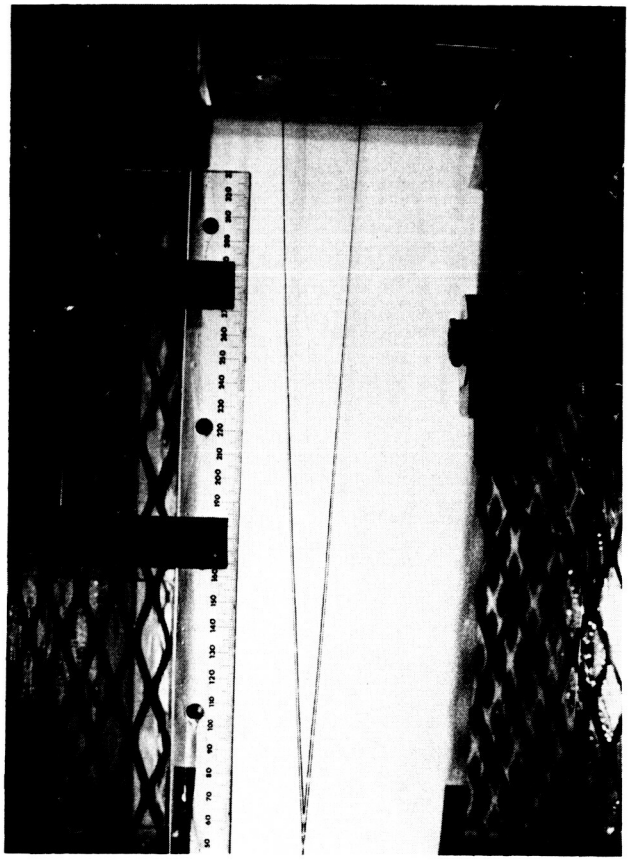

(A) (d_0= 109 μM, ℓ/d_0 = 3.44, L/W = 9.6, V_0 = 11.1 M/S).

FIGURE 5. - CONVERGENCE OF A 34 MM WIDE SHEET.

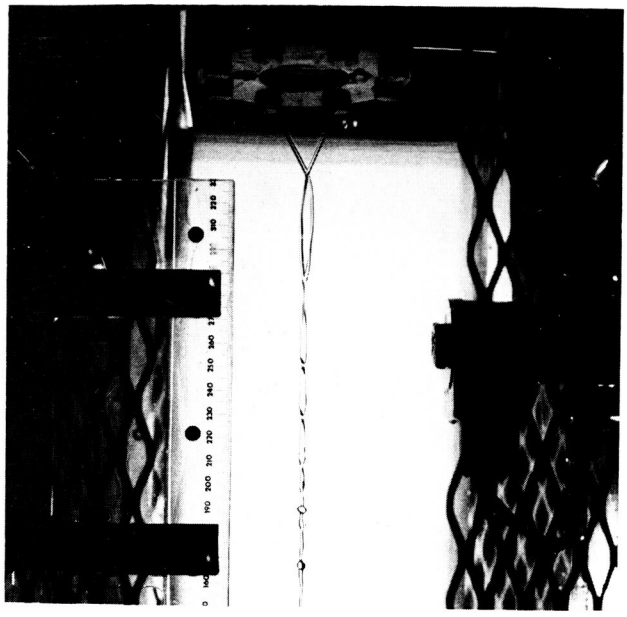

(B) (d_0 = 109 μm, ℓ/d_0 = 3.44, L/w = 1.5, V_0 1.75 m/s).

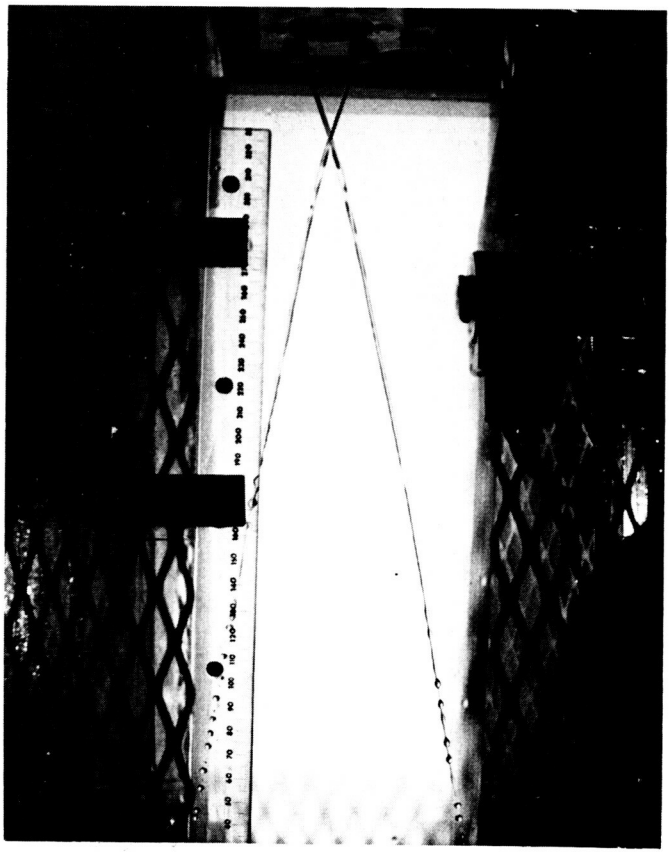

(C) (d_0 = 114 μm, ℓ/d_0 = 1.0, L/w = 1.6, V_0 = 2.13 m/s).

FIGURE 5. - CONCLUDED.

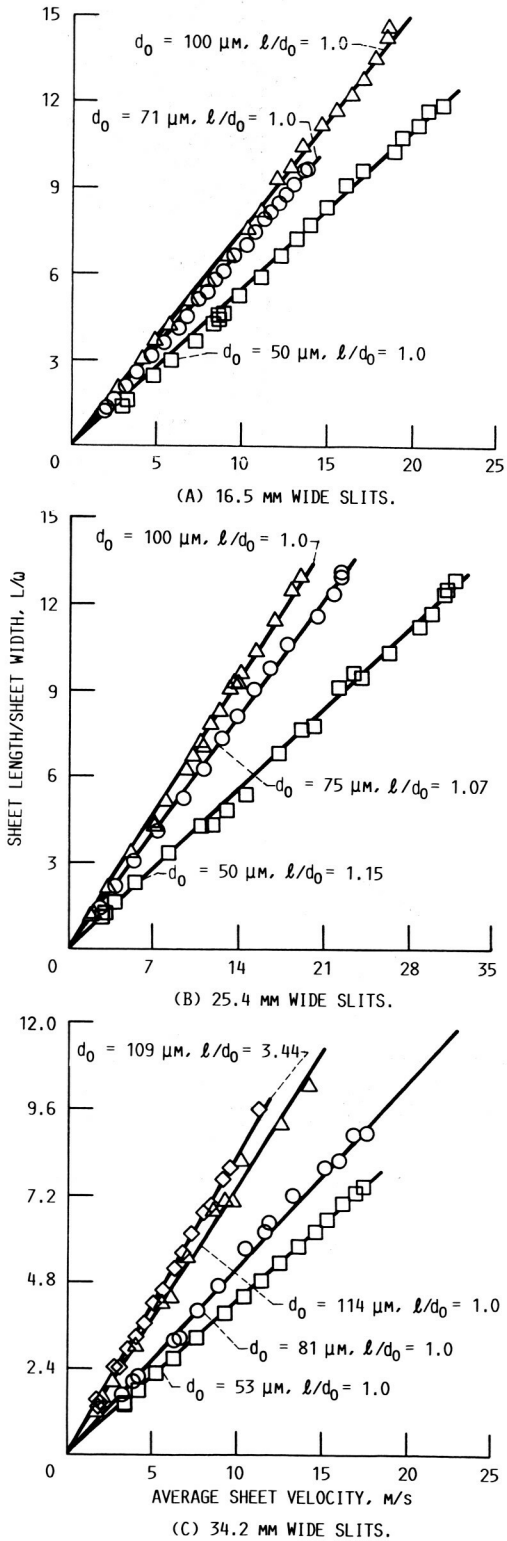

FIGURE 6. - DIMENSIONLESS SHEET LENGTH.

1. Report No.	2. Government Accession No.	3. Recipient's Catalog No.
NASA TM-89841		

4. Title and Subtitle	5. Report Date
Liquid Sheet Radiator	
	6. Performing Organization Code: 506-41-5A

7. Author(s)	8. Performing Organization Report No.
Donald L. Chubb and K. Alan White, III	E-3497
	10. Work Unit No.

9. Performing Organization Name and Address	11. Contract or Grant No.
National Aeronautics and Space Administration Lewis Research Center Cleveland, Ohio 44135	
	13. Type of Report and Period Covered: Technical Memorandum
12. Sponsoring Agency Name and Address	14. Sponsoring Agency Code
National Aeronautics and Space Administration Washington, D.C. 20546	

15. Supplementary Notes

Prepared for the 22nd Thermophysics Conference sponsored by the American Institute of Aeronautics and Astronautics, Honolulu, Hawaii, July 8-10, 1987.

16. Abstract

A new external flow radiator concept, the liquid sheet radiator (LSR), is introduced. The LSR sheet flow is described and an expression for the length/width L/w, ratio is presented. A linear dependence of L/w on velocity is predicted that agrees with experimental results. Specific power for the LSR is calculated and is found to be nearly the same as the specific power of a liquid droplet radiator, (LDR). Several sheet thicknesses and widths were experimentally investigated. In no case was the flow found to be unstable.

17. Key Words (Suggested by Author(s))	18. Distribution Statement
Liquid sheet radiator Sheet flow External flow radiator	Unclassified - unlimited STAR Category 34

19. Security Classif. (of this report)	20. Security Classif. (of this page)	21. No. of pages	22. Price*
Unclassified	Unclassified	11	A02

*For sale by the National Technical Information Service, Springfield, Virginia 22161